Tunneling between two two-dimensional electron systems in a strong magnetic field

Peter Johansson and Jari M. Kinaret
NORDITA, Blegdamsvej 17, DK-2100 Copenhagen Ø, Denmark
(Received 4 January 1994; revised manuscript received 30 March 1994)

We calculate the tunnel current between two parallel two-dimensional electron systems in a strong perpendicular magnetic field. We model the strongly correlated electron systems by Wigner crystals and describe their low-energy dynamics in terms of magnetophonons. The effects of the magnetophonons on the tunneling processes can be described by an exactly solvable independent-boson model. A tunneling electron shakes up magnetophonons, which results in a conductance peak that is displaced away from zero voltage and broadened compared with the case of no magnetic field. At low temperatures and low enough voltages the tunneling conductance is strongly suppressed and the I-V characteristics exhibit a power-law behavior. We also analyze the effects of excitation of magnetoplasmons, which have a gap equal to the cyclotron energy and therefore give rise to a second peak in the I-V curves. Most of our results are in good quantitative agreement with the recent experiments by Eisenstein, Pfeiffer, and West [Phys. Rev. Lett. **69**, 3804 (1992)].

I. INTRODUCTION

The quantum Hall effect, and more generally the physics of electrons in a strong magnetic field, have been studied intensively for more than ten years. Quite naturally, most of the experimental effort has concentrated on measurements of lateral transport properties, such as the Hall resistance. In recent years, however, a few experiments measuring the tunnel current in or out of the two-dimensional (2D) electron systems, subject to a strong perpendicular magnetic field, have been performed.

Ashoori *et al.*[1] studied the tunneling between a 2D electron system in a quantum well and a 3D doped substrate. They found that the low-voltage tunnel conductance was reduced in a strong magnetic field. Eisenstein, Pfeiffer, and West[2] measured the tunnel conductance between two parallel 2D electron systems in a perpendicular magnetic field, which was strong enough that only the lowest Landau level was partially filled. They found effects of the magnetic field in the I-V characteristics of their tunnel junction that resembled the Coulomb blockade effect.[3] The I-V curve showed a pseudogap, i.e., a finite voltage was needed before any appreciable tunnel current could flow between the electron systems. The tunnel current as a function of voltage exhibited a maximum at a voltage roughly corresponding to the electrostatic energy $e^2/4\pi\epsilon\langle a\rangle$ of a pair of electrons separated by the typical interelectron spacing $\langle a\rangle$ in the 2D electron systems (e is the elementary charge and ϵ is the dielectric constant of the material). The suppression of the small-bias conductance was sensitive to the temperature; it showed an activated behavior and the experimentally observed activation temperature was typically ~ 10 K.

In this paper, we present a model calculation aimed at explaining the essential findings of the experiment by Eisenstein, Pfeiffer, and West.[2] A short account of our work has been published previously.[4] The strong suppression of the tunnel current for small-bias voltages is, as we understand it, a result of strong correlations between the electrons in the two 2D systems in the presence of a strong perpendicular magnetic field B. The electrons behave as wave packets whose size is set by the magnetic length $l_c = (\hbar/eB)^{1/2}$. The motion of these wave packets is correlated, therefore, when a tunneling event takes place, a local perturbation is created. When the electron systems attempt to relax back to their ground states, energy is carried away in the form of collective excitations. A tunneling event is usually a much faster process than the relaxation mechanisms in the electron systems, so we can analyze the process within the sudden approximation. The state of the electron system immediately after a tunneling event has a very small overlap with the ground state. This is characteristic of an orthogonality catastrophe.[5,6] The only way of getting states of the electron systems that have large overlaps with the suddenly created state is by introducing many low-energy excitations. Thus, the scenario is the same as in the x-ray edge problem where a core hole is suddenly created inside an electron gas. In response to this, many low-energy electron-hole pairs are excited in the electron gas. In the theory we present here, the tunneling electron and the "vacancy" it leaves behind play the same role as the core hole does in the x-ray edge problem. Similar ideas have been used to explain the effects of quantum fluctuations in the "ordinary" Coulomb blockade.[7–9]

To calculate quantities that can be compared with experiment we need a model for the 2D electron systems. We have chosen to approximate them by Wigner crystals. This gives, as we will see, a reasonable description of the short-range correlations in the real electron systems, and has the advantage that the low-energy collective excitations are easy to describe. A Wigner crystal has gapless collective excitations, called magnetophonons, which play the most important part in the relaxation processes that we will discuss. Thus, with the Wigner-crystal model we can write down an exactly solvable Hamilto-

nian in which all parameters can be calculated from first principles.

The results of our calculation agree very well with the experiment[2] on all the three points mentioned above: (i) We find that the conductance at low voltage and temperature is strongly suppressed. For small voltages the current is approximately given by a power law, $I \sim V^{\gamma}$, where typically $\gamma \approx 5$–10. (ii) The tunnel current exhibits a broad maximum around the peak voltage $V_{\rm peak}$. Theoretically, we find that $V_{\rm peak}$ is approximately given by

$$V_{\rm peak} \approx 2\frac{e}{4\pi\epsilon\langle a\rangle}. \tag{1}$$

This is in close agreement with the experiment.[2] (iii) When we vary the temperature in our calculation we find an activated behavior of the zero-bias conductance. The values of the activation temperature show the same kind of dependence on the magnetic field as in the experiment and the absolute values do not differ by more than $\approx 20\%$.

A number of other theories addressing these experiments[1,2] have been presented recently. Hatsugai, Bares, and Wen[10] calculated the one-electron spectral function of a finite electron system in a strong magnetic field by an exact numerical diagonalization, and discussed their results in terms of selection rules. A similar calculation was done by He, Platzman, and Halperin.[11] The tunnel current is proportional to the convolution of the spectral function associated with the addition of an electron and the spectral function associated with the removal of an electron. Due to the finite size of the systems used in these calculations it is not possible to get continuous results for the tunnel current, but both calculations seem to predict a peak in the tunnel current at about the same voltage as in the experiment. The authors of Ref. 11 also presented analytic results for the tunnel current in the limit of a small voltage. In doing this, they mapped the tunneling problem onto the x-ray edge problem, in a way similar to what we do here. The collective excitations shaken up by the tunneling event in their theory were density fluctuations in a Chern-Simons Fermi liquid.[12] Yang and MacDonald[13] calculated the tunneling density of states of a 2D electron system in a strong magnetic field also taking rather strong disorder into account. They found a suppression of the tunneling conductance at small voltages, but no (pseudo)gap. Their calculation is most likely primarily applicable to the experiment by Ashoori *et al.*,[1] since the samples used there had much lower mobilities than the ones used by Eisenstein, Pfeiffer, and West.[2] Finally, Efros and Pikus[14] have studied a lattice-gas model of an essentially classical electron liquid using Monte Carlo methods.

The rest of this paper is organized in the following way. In Sec. II, we present and discuss our model. We calculate the magnetophonon frequencies of the model Wigner crystal, and the matrix elements that couple the tunneling electrons to the magnetophonons. In Sec. III we calculate the tunnel current between the two electron systems including effects of magnetophonon shakeup. We also present numerical results for the current as a function of the magnetic field, the temperature, and the electron density. The measured tunnel current[2] exhibits an additional peak associated with excitations to the next Landau level. In Sec. IV, we extend our theory to also take into account this effect. Section V contains a discussion and evaluation of our results. The main text is ended by a short summary in Sec. VI. In Appendix A, we give rapidly converging expressions for the dynamical matrix of the Wigner crystal. To arrive at a second-quantized form of the magnetophonon Hamiltonian one must perform a canonical transformation, which we describe in Appendix B. The implications of our model for the I-V characteristics at very low voltages are discussed in Appendix C.

II. THE MODEL

The two-dimensional electron systems studied in the experiment by Eisenstein, Pfeiffer, and West[2] were in a strong perpendicular magnetic field. Only the lowest Landau level was partially filled, i.e., the filling factor ν was less than one. The kinetic energy of such a system is quenched, and the motion of the electrons is inevitably strongly correlated. The single-electron states can be thought of as Gaussian wave packets with a linear size of the order of the magnetic length. All these states have the same energy; the creation of a single-particle excitation requires an amount of energy equal to the cyclotron energy

$$\hbar\omega_c = \frac{\hbar eB}{m^*}, \tag{2}$$

where B is the magnetic field and m^* is the electron effective mass. Thus, the low-energy dynamics is governed by the potential energy. The electron wave packets try to avoid each other so the 2D electron systems are most likely in strongly correlated, compressible, liquid states, or, for very small filling factors ($\nu \lesssim 1/6$), in a Wigner-crystal state.

In a tunneling event an electron is suddenly brought from one of these liquids into the other leading to rearrangements in both systems. In one quantum well "resident" electrons must fill the empty space left behind by the tunneling electron, while in the other well they are pushed aside by the newly appeared tunneling electron. When these rearrangements take place, energy is carried away in the form of collective excitations in the electron liquids. In our view, this is the fundamental reason for the fact that the tunnel current and conductance both have maxima at finite-bias voltages, and are strongly suppressed at zero voltage. The energy lost in relaxation processes must be provided by the external voltage source.

Let us contrast this to the situation with no perpendicular magnetic field. Then the electron motion parallel to the barrier is essentially free, and the single-electron states are extended over a large area. Consequently, a tunneling event does not lead to any appreciable changes

in the correlation energies of the other electrons. Thus, the I-V characteristics are determined by the fact that the electron momentum parallel to the barrier, as well as the energy, is conserved in each tunneling event. This leads to a tunneling conductance that shows a sharp peak at zero bias.[2] The small width of this peak is caused by processes in which parallel momentum is not conserved, such as impurity and interface-roughness scattering.[15]

In the subsequent calculations we model the 2D electron systems as triangular Wigner crystals with a lattice parameter a_0 set by the electron density of the 2D electron systems, see Fig. 1. This clearly takes the picture of the correlated electron liquids one step further towards stronger correlation. We believe that the Wigner crystals give rather a good description of the actual electron systems on short length scales (at least up to a few lattice parameters). The great advantage gained by using this picture is that we can write down an exactly solvable Hamiltonian in which all quantities can be calculated from first principles, and moreover we get results in the thermodynamic limit. Due to the periodicity of the Wigner crystal the collective oscillations, the magnetophonons and magnetoplasmons, can be calculated rather easily.

As a first approximation the experimentally observed Coulomb blockade can be explained as the difference in Madelung energy between a lattice site (initial state) and an interstitial site (final state) of the Wigner crystals, see Fig. 1. This would move the sharp conductance peak one sees for $B = 0$ out to a finite voltage. To get a broadened conductance peak we must also take into account the quantum fluctuations in the dynamics of the Wigner crystal. This is done by coupling to magnetophonons and magnetoplasmons.

We have calculated the magnetophonon frequencies classically within the harmonic approximation.[16] Let $\mathbf{u}_i$ denote the displacement of the electron at the lattice point $\mathbf{R}_i$ and introduce its Fourier transform by

$$\mathbf{u}_i = \frac{1}{\sqrt{N}} \sum_{\mathbf{q}} \mathbf{u}_{\mathbf{q}}\, e^{i\mathbf{q}\cdot\mathbf{R}_i}, \tag{3}$$

where N is the total number of electrons in the Wigner crystal. Using classical mechanics we see that a solution developing harmonically in time, $\mathbf{u}_{\mathbf{q}}(t) = \mathbf{u}_{\mathbf{q}} e^{-i\omega_{\mathbf{q}} t}$, must satisfy the equation of motion

$$-\omega_{\mathbf{q}}^2 \mathbf{u}_{\mathbf{q}} + i\omega_{\mathbf{q}}\omega_c \mathbf{u}_{\mathbf{q}} \times \hat{z} + \widehat{D}(\mathbf{q})\mathbf{u}_{\mathbf{q}} = 0. \tag{4}$$

Here $\widehat{D}(\mathbf{q})$ is the dynamical matrix (from now on we denote matrices with a caret) which we define and evaluate in Appendix A. To get nontrivial solutions to the equation of motion the determinant

$$\begin{vmatrix} \omega_{T\mathbf{q}}^2 - \omega_{\mathbf{q}}^2 & i\omega_c\omega_{\mathbf{q}} \\ -i\omega_c\omega_{\mathbf{q}} & \omega_{L\mathbf{q}}^2 - \omega_{\mathbf{q}}^2 \end{vmatrix}$$

must vanish. Here $\omega_{T\mathbf{q}}$ and $\omega_{L\mathbf{q}}$ are the transverse and longitudinal phonon frequencies of the Wigner crystal in the absence of any magnetic field. The squares of these frequencies are the eigenvalues of the dynamical matrix. For small $\mathbf{q}$ we find that $\omega_{T\mathbf{q}} \sim |\mathbf{q}|$, while the longitudinal phonons, being 2D plasmons, exhibit the long-wavelength dispersion relation $\omega_{L\mathbf{q}} \sim \sqrt{|\mathbf{q}|}$, as can be seen from Eq. (A3).

In a magnetic field the transverse and longitudinal modes get mixed: when a magnetophonon or magnetoplasmon propagates through the Wigner crystal each individual electron moves along an elliptic path, see Fig. 2. The longitudinal phonons develop into magnetoplasmons. This mode has a gap equal to the cyclotron energy $\hbar\omega_c$. The transverse phonons become magnetophonons. This mode is gapless, also with a magnetic field present. Therefore, the low-energy dynamics of a Wigner crystal is determined by the magnetophonons. In the long-wavelength limit the magnetophonon frequency behaves as

$$\omega_{\mathbf{q}} \approx \frac{\omega_{T\mathbf{q}}\omega_{L\mathbf{q}}}{\omega_c} \sim |\mathbf{q}|^{3/2}. \tag{5}$$

Another remarkable property of the magnetophonons is that their frequencies, in the limit of a strong magnetic field (i.e., when $\omega_c \gg \omega_{\mathbf{q}}$), are independent of the electron

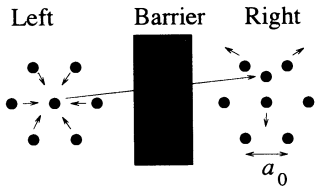

FIG. 1. Schematic picture of a tunneling event in our model. An electron starts from a lattice position in one of the triangular Wigner crystals (for clarity these have been depicted in a top view) and ends up in an interstitial position on the other side of the barrier. The surrounding electrons experience a sudden change in the potential and as a result relaxation processeses take place in the electron systems on both sides of the barrier. In our model the energy released in these relaxation processes is carried away mainly in the form of magnetophonons.

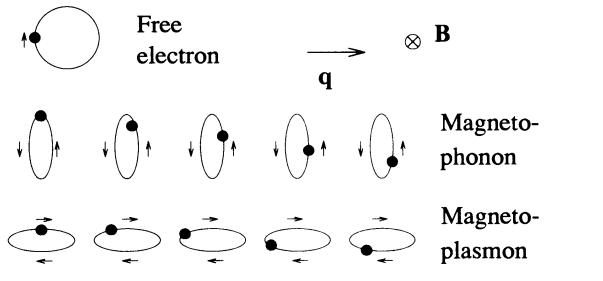

FIG. 2. Qualitative illustration of magnetophonon and magnetoplasmon waves. The electrons move classically along elliptic paths as the different waves propagate. The magnetophonon is mostly a transverse excitation. Here the electrons rotate in the opposite direction compared with a free electron in a magnetic field. When a magnetoplasmon propagates the electrons rotate in the same direction as a free electron. The magnetoplasmon is mainly longitudinal, but we have exaggerated the eccentricity of the magnetoplasmon ellipses in this figure.

mass. The motion of a magnetophonon is determined by requiring that the Lorentz force and the electrostatic, restoring forces balance each other. Since the restoring forces are proportional to the second derivative of the Coulomb potential, a dimensional analysis shows that the magnetophonon frequencies behave as

$$\omega_{\mathbf{q}} \sim \frac{1}{a_0^3 B}. \tag{6}$$

In Fig. 3, we give the full dispersion relation of the magnetophonons along the edge of the irreducible Brillouin zone in a few typical cases in order to illustrate the points above.

Côté and MacDonald[17] have calculated the magnetophonon frequencies of a Wigner crystal going beyond the harmonic approximation. They used a time-dependent Hartree-Fock approximation and could capture quantum-mechanical effects. Their calculation only assumes that the electron density of the ground state is periodic, but the electrons are free to move itinerantly between different unit cells. We find that even though the dispersion relations found by us, and in Ref. 17, differ somewhat in details, the qualitative differences are not very large, at least not for moderate filling factors. We conclude that for our present purposes it is sufficient to treat the magnetophonons within the harmonic approximation.

It is more difficult to say how well the magnetophonons approximate the collective modes of the real experimental system. We think it is reasonable to say that the calculation in Ref. 17 should give results that describe the short-wavelength modes, also in an electron liquid, fairly well. From the comparison in the paragraph above we see that our calculation also should give reasonable results in that wavelength regime. It is less clear what happens to the long-wavelength magnetophonons when going from a crystal to a correlated liquid ground state. An electron liquid in a strong magnetic field can support long-wavelength transverse oscillations because the Lorentz force couples longitudinal and transverse degrees of freedom. This means that some collective mode reminiscent of the magnetophonons should persist in the liquid state.

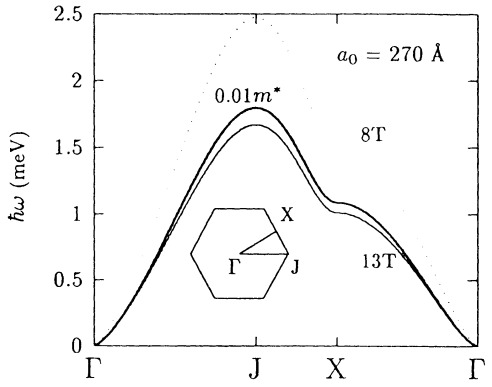

FIG. 3. The magnetophonon dispersion relation along the edges of the irreducible Brillouin zone (inset). The upper curve is for a magnetic field of 8 T, while the two lower curves are for 13 T. The thick curve has been calculated using an electron mass that is 100 times too small, to show that electron inertia is of practically no importance to the magnetophonon frequencies.

Finally, we must include an interaction between the tunneling electron and the magnetophonons in our model. Our calculation of these electron-magnetophonon matrix elements is similar to the calculation of electron-phonon matrix elements in ordinary solids.[18] Thus, the Coulomb interaction between the added, or removed, tunneling electron and the Wigner-crystal electrons is expanded to linear order in the displacements $\mathbf{u}_i$. Further details are given in Appendix B.

The above considerations lead us to use the following model Hamiltonian:

$$H = H_0 + H_T^+ + H_T^- = \left[\varepsilon_L + \sum_\alpha (M_{\alpha L} a_\alpha + M_{\alpha L}^* a_\alpha^\dagger)\right] c_L^\dagger c_L + \left[\varepsilon_R + \sum_\alpha (M_{\alpha R} a_\alpha + M_{\alpha R}^* a_\alpha^\dagger)\right] c_R^\dagger c_R + \sum_\alpha \hbar\omega_\alpha a_\alpha^\dagger a_\alpha + T_{LR} c_R^\dagger c_L + T_{LR}^* c_L^\dagger c_R. \tag{7}$$

In writing down this Hamiltonian we focus our attention to an area $2\pi l_c^2$. This area holds exactly one electron state in the lowest Landau level in each of the quantum wells. The operator $c_{L(R)}$ destroys an electron in the left (right) well, and $\varepsilon_{L(R)}$ is the corresponding site energy. This energy depends on how the surrounding Wigner crystal is arranged. We can think of $\varepsilon_{L(R)}$ as the Madelung energy of an electron in either a lattice position or an interstitial position of the Wigner crystal. The matrix element $M_{\alpha L(R)}$ gives the interaction between magnetophonon mode α and the tunneling electron when it is in the left (right) quantum well. The symbol α is a composite index denoting both what wave vector a magnetophonon has and in which quantum well it propagates. The magnetophonon frequencies ω_α are found in the calculation described above; however, to get the second-quantized form of the Hamiltonian it is necessary to perform a canonical transformation[19] which we describe in Appendix B.

The last two terms (H_T^+ and H_T^-) allow an electron to tunnel between the quantum wells. We have calculated the tunneling matrix element T_{LR} following the method of Bardeen.[20] In terms of the quantum well width L, the barrier height V_b, and width d, we get

$$T_{LR} = \frac{\hbar^2}{m_b} \frac{\cos^2(kL/2)\kappa e^{-\kappa d}}{L/2 + \sin(kL)/(2k) + \cos^2(kL/2)/\kappa}, \tag{8}$$

where $k = \sqrt{2m^*E/\hbar^2}$ and $\kappa = \sqrt{[2m_b(V_b - E)]/\hbar^2}$. Here E denotes the eigenenergy of the lowest bound state in a quantum well. It is found from the equation

$$\frac{k}{m^*}\tan(kL/2) = \frac{\kappa}{m_b}. \tag{9}$$

In our calculations we set the electron effective masses in the barrier and the wells equal to each other, $m_b = m^* = 0.067m_e$. Thus, the Hamiltonian (7) contains no adjustable parameters.

The separation of the 2D electron systems into a small area in which electrons are treated as fermions and are allowed to tunnel between the wells, and a large area in which the electron dynamics can be treated in terms of bosonic degrees of freedom, is of course purely formal. Tunneling events take place over the entire area of the sample; when we calculate the total tunnel current we must sum over the total sample area. The physical implication of the formal separation is that tunneling events at different places of the sample can be treated as independent of each other. To support this statement we note that in the experiment the tunnel current was typically 3 nA, which corresponds to one tunneling event every 50 ps. On the other hand, the period of oscillation of a typical collective excitation of the Wigner crystals is about 4 ps (corresponding to an energy of 1 meV). More importantly, the magnetophonons decay through emission of *lattice* acoustic phonons; the phase velocity of the magnetophonons is larger than the speed of sound in GaAs (5200 m/s) practically everywhere in the Wigner-crystal Brillouin zone. A free electron in GaAs is thermalized by acoustic phonons on a time scale shorter than 1 ns. While the rate of acoustic-phonon emission by a magnetophonon in a Wigner crystal most likely is modified compared with the free-electron case, 1 ns should be a reasonable estimate of the thermalization time scale. Thus, at each time the Wigner crystal has magnetophonon excitations originating from not more than 100 tunneling events. This corresponds to an energy of $\approx$1 eV, and is negligible since the experimental system contained $\approx 10^8$ electrons in each well.

Let us in this context also point out that it is justified to treat the electron tunneling as an instantaneous event. This simplifies the treatment considerably, but we note that theories in which tunneling electrons interact with other degrees of freedom with response times comparable to the tunneling time have been developed.[21,22] We calculate the time it takes for an electron to traverse an inverted 250-meV barrier which is 175 Å thick (instanton approximation) to be $\approx$ 15 fs. Thus, the parameter values of the experiment give a tunneling time that is more than two orders of magnitude shorter than the typical period of a magnetophonon oscillation.

We end this section by discussing an important feature of the model. The electron-magnetophonon interaction in Eq. (7) only changes the state of the magnetophonon system, while the electron stays in the same state as before the interaction, i.e., it does not recoil. Consequently the different magnetophonon emissions are independent of each other since earlier events do not affect the electron. The model is, therefore, called an independent-boson model, and it is exactly solvable. Independent-boson models have often been used to describe relaxation processes in solid-state physics. The x-ray edge problem[23,24] (the interaction between a heavy core hole and an electron gas) is the best known case, but quite a number of other examples exist: effects of quantum fluctuations on the ordinary Coulomb blockade,[8,9] electron energy loss spectroscopy,[25] and LO phonon scattering in resonant tunneling[26] to mention a few. We think it is reasonable to use the independent-boson model in the present calculation. While the electron by no means is an infinitely heavy object, in a strong magnetic field it can be described as a fairly localized wave packet, which behaves as a rather rigid object. It should, therefore, be justified to neglect recoil effects.

III. THE TUNNEL CURRENT

A. Formalism

The barrier through which the electron tunnels is rather thick. It, therefore, suffices to calculate the tunnel current to lowest order in the tunneling terms H_T^+ and H_T^- of the Hamiltonian. The Fermi golden rule gives immediately

$$I(V) = e\frac{2\pi}{\hbar}\sum_{i,f}\frac{e^{-\varepsilon_i/k_BT}}{Z}\Big[|\langle \mathrm{f}|H_T^+|\mathrm{i}\rangle|^2\delta(\varepsilon_i-\varepsilon_f+eV) - |\langle \mathrm{f}|H_T^-|\mathrm{i}\rangle|^2\delta(\varepsilon_i-\varepsilon_f-eV)\Big], \tag{10}$$

where $|\mathrm{i}\rangle$ and $|\mathrm{f}\rangle$ are the initial and final states and ε_i and ε_f are their respective eigenenergies (of H_0), Z, finally, is the partition function. In practice we restrict the thermal averaging to the magnetophonon degrees of freedom, higher electronic states are frozen out at the temperatures we consider. The first term gives the forward current (from left to right), while the second term gives the backward current. The δ functions can be transformed into time integrals; this yields

$$I(V) = \frac{e}{\hbar^2}\int_{-\infty}^{\infty}dt\Big[e^{ieVt/\hbar}\langle H_T^-(t)H_T^+(0)\rangle - e^{-ieVt/\hbar}\langle H_T^+(t)H_T^-(0)\rangle\Big]. \tag{11}$$

The equivalence between Eq. (10) and Eq. (11) is easily seen if one inserts $H_T^\pm(t) = e^{iH_0t/\hbar}H_T^\pm e^{-iH_0t/\hbar}$ into Eq. (11).

Thus, to calculate the current we need to evaluate the correlation functions $I^{-+}(t) = \langle H_T^-(t)H_T^+(0)\rangle$ and $I^{+-}(t) = \langle H_T^+(t)H_T^-(0)\rangle$. The Hamiltonian H_0 is an exactly solvable independent-boson model, so this evaluation can be done in many different ways, see Ref. 27. Here we will use an exponential resummation (linked cluster expansion). Let us concentrate on one of the correlation functions

$$I^{-+}(t) = |T_{LR}|^2\langle e^{iH_0t/\hbar}c_L^\dagger c_R e^{-iH_0t/\hbar}c_R^\dagger c_L\rangle. \tag{12}$$

We proceed by noticing that the operator H_0 can be replaced by two different specific expressions at the two places where it appears,

$$I^{-+}(t) = |T_{LR}|^2 \langle e^{iH_i t/\hbar} c_L^\dagger c_R e^{-iH_f t/\hbar} c_R^\dagger c_L \rangle. \tag{13}$$

These initial and final Hamiltonians, which describe the system before and after the tunneling event, are

$$H_i = \varepsilon_L + \sum_\alpha \hbar\omega_\alpha a_\alpha^\dagger a_\alpha + \sum_\alpha (M_{\alpha L} a_\alpha + M_{\alpha L}^* a_\alpha^\dagger), \tag{14a}$$

and

$$H_f = \varepsilon_R + \sum_\alpha \hbar\omega_\alpha a_\alpha^\dagger a_\alpha + \sum_\alpha (M_{\alpha R} a_\alpha + M_{\alpha R}^* a_\alpha^\dagger). \tag{14b}$$

We proceed by inserting $e^{-iH_i t/\hbar} e^{iH_i t/\hbar} = 1$ into Eq. (13) which yields

$$I^{-+}(t) = |T_{LR}|^2 \langle e^{iH_i t/\hbar} c_L^\dagger c_R e^{-iH_i t/\hbar}\ e^{iH_i t/\hbar} e^{-iH_f t/\hbar}\ \ c_R^\dagger c_L \rangle. \tag{15}$$

No electron operators appear neither in H_i nor in H_f, so the electron contribution to the correlation function is only the product of the number of available electrons in the left well times the number of empty states in the right well, $\nu(1-\nu)$. This means that we assume that the two Wigner crystals are mutually completely uncorrelated. Since some correlations most likely exist, the factor $(1-\nu)$ should be replaced by a larger number (still smaller than 1, though), but as we do not have a good way of estimating this number we keep $(1-\nu)$ in our equations. We are left with the magnetophonon contribution $\langle e^{iH_i t/\hbar} e^{-iH_f t/\hbar} \rangle$, which is equal to the time-development operator in the interaction representation of H_i due to the perturbation $H_f - H_i$. Thus,

$$I^{-+}(t) = \nu(1-\nu)|T_{LR}|^2 \langle e^{iH_i t/\hbar} e^{-iH_f t/\hbar} \rangle = \nu(1-\nu)|T_{LR}|^2 \left\langle \mathrm{T} \exp\left[-\frac{i}{\hbar} \int_0^t dt' \hat{V}(t') \right] \right\rangle, \tag{16}$$

where

$$\hat{V}(t) = e^{iH_i t/\hbar} (H_f - H_i) e^{-iH_i t/\hbar}, \tag{17}$$

and T is a time-ordering operator. It turns out that the expectation value appearing in Eq. (16) can be calculated exactly by an exponential resummation collecting the first two cumulants.[27] This yields the final result for the correlation function

$$I^{-+}(t) = \langle H_T^-(t) H_T^+(0) \rangle = \nu(1-\nu)|T_{LR}|^2 C(t), \tag{18}$$

where

$$C(t) = e^{i(\varepsilon_L - \Delta_L - \varepsilon_R + \Delta_R)t/\hbar} \exp\Big(-\sum_\alpha \frac{|M_{\alpha R} - M_{\alpha L}|^2}{(\hbar\omega_\alpha)^2} [(1+N_\alpha)(1-e^{-i\omega_\alpha t}) + N_\alpha (1-e^{i\omega_\alpha t})] \Big). \tag{19}$$

Here N_α denotes the thermal occupation of magnetophonon mode α, $N_\alpha = [\exp(\hbar\omega_\alpha/k_B T) - 1]^{-1}$. We have also introduced the "polaron shifts" $\Delta_{L(R)}$, which are defined by

$$\Delta_{L(R)} = \sum_\alpha \frac{|M_{\alpha L(R)}|^2}{\hbar\omega_\alpha}. \tag{20}$$

The polaron shifts simply tell how much energy the Wigner crystals can gain by relaxing to the new ground state when subject to the external perturbation implied by the electron-magnetophonon interaction. In the following, we will just set the exponential prefactor in Eq. (19) equal to unity. This means that we assume the polaron shift cancels the difference between the lattice position and interstitial Madelung energies. Physically this means that the Wigner crystals can relax completely after a tunneling event. The calculations of Madelung energies that we have made indicate that this approximation is accurate, and it means that the threshold voltage for tunneling is zero.

If instead tunneling from right to left is considered, we find an identical expression for the correlation function $\langle H_T^+(t) H_T^-(0) \rangle$. Thus, by performing the integrals in Eq. (11) we get the following final result for the tunnel current,

$$I(V) = \frac{S}{2\pi l_c^2} \frac{e}{\hbar^2} \nu(1-\nu)|T_{LR}|^2 [C(eV/\hbar) - C(-eV/\hbar)]. \tag{21}$$

To get this expression we have summed over the entire area S of the sample, assuming that the tunneling events at different places are independent of each other.

Before we are done, we must evaluate the Fourier transform $C(\omega)$. Since $C(t)$ is a complicated function of time,

it is difficult to do this by means of direct integration. We will instead use the integral-equation method due to Minnhagen.[24] Let us first look at the case of zero temperature. Then $N_\alpha = 0$, and it is easy to see that [remember that the first exponential in (19) is unity]

$$C(\omega) = 0 \quad \text{for} \quad \omega < 0. \tag{22}$$

Moreover, $C(t = 0) = 1$, which gives the normalization condition

$$\int_0^\infty \frac{d\omega}{2\pi} C(\omega) = 1. \tag{23}$$

To derive an integral equation for $C(\omega)$ we calculate the time-derivative $C'(t)$,

$$C'(t) = -i \sum_\alpha \frac{|M_{\alpha R} - M_{\alpha L}|^2}{\hbar^2 \omega_\alpha} e^{-i\omega_\alpha t} C(t). \tag{24}$$

Fourier transforming this equation we obtain

$$\omega C(\omega) = \int_0^{\omega_{\max}} \frac{d\Omega}{2\pi} g(\Omega) C(\omega - \Omega), \tag{25}$$

where we have introduced

$$g(\Omega) = 2\pi \sum_\alpha \frac{|M_{\alpha R} - M_{\alpha L}|^2}{\hbar^2 \Omega} \delta(\Omega - \omega_\alpha), \tag{26}$$

and $\omega_{\max}$ is the maximum magnetophonon frequency. Now it is easy to calculate $C(\omega)$ from Eq. (25) numerically. We calculate $C(\omega)$ for increasing frequencies, and to do this we only need to know $C(\omega)$ at lower frequencies, where it has already been calculated.

At a finite temperature the integral-equation method still works provided that it is divided into two steps. First we notice that $C(t)$ can be factorized into an emission and an absorption part,

$$C(t) = C_{\text{em}}(t) C_{\text{abs}}(t), \tag{27}$$

where

$$C_{\text{em}}(t) = \exp\Big(- \sum_\alpha \frac{|M_{\alpha R} - M_{\alpha L}|^2}{(\hbar\omega_\alpha)^2} \times [(1 + N_\alpha)(1 - e^{-i\omega_\alpha t})] \Big), \tag{28a}$$

and

$$C_{\text{abs}}(t) = \exp\Big(- \sum_\alpha \frac{|M_{\alpha R} - M_{\alpha L}|^2}{(\hbar\omega_\alpha)^2} N_\alpha (1 - e^{i\omega_\alpha t}) \Big). \tag{28b}$$

We now find that $C_{\text{em}}(\omega)$ satisfies

$$\omega C_{\text{em}}(\omega) = \int_\delta^{\omega_{\max}} \frac{d\Omega}{2\pi} g(\Omega)[1 + N(\Omega)] C_{\text{em}}(\omega - \Omega), \tag{29}$$

along with the conditions $C_{\text{em}}(\omega) = 0$ for $\omega < 0$, and $\int_0^\infty d\omega C_{\text{em}}(\omega)/2\pi = 1$. In Eq. (29), $N(\Omega)$ is the thermal occupation of a harmonic oscillator, $N(\Omega) = [\exp(\hbar\Omega/k_B T) - 1]^{-1}$. The expressions determining $C_{\text{abs}}(\omega)$ are

$$\omega C_{\text{abs}}(\omega) = - \int_\delta^{\omega_{\max}} \frac{d\Omega}{2\pi} g(\Omega) N(\Omega) C_{\text{abs}}(\omega + \Omega), \tag{30}$$

while $C_{\text{abs}}(\omega) = 0$ for $\omega > 0$, and $\int_{-\infty}^0 d\omega C_{\text{abs}}(\omega)/2\pi = 1$. Note that we have introduced a cutoff δ in the frequency integrals to deal with the fact that $N(\Omega)$ diverges as $1/\Omega$. This can be viewed as taking a principal value. It does not affect the final results as long as one uses the same, small δ in both the integral equations. At this point, as a consequence of Eq. (27), we find $C(\omega)$ through a frequency convolution,

$$C(\omega) = \int_0^\infty \frac{d\omega'}{2\pi} C_{\text{em}}(\omega') C_{\text{abs}}(\omega - \omega'). \tag{31}$$

B. Results

The basic results of this section are presented in Fig. 4, where we have plotted the tunnel current as a function of bias voltage for a number of different magnetic fields. All parameter values, regarding electron density, barrier height and thickness, quantum well width, etc., used in the calculation have been taken from the experiment of Eisenstein, Pfeiffer, and West;[2] for comparison we also display a plot of their results in Fig. 4(b). The qualitative behavior of the theoretical I-V curves is the same as in the experiment. For small voltages the current is strongly suppressed; it then has a relatively broad peak centered around 8–10 meV. The peak voltages that we find agree rather well with those found experimentally. Experimentally the peak voltage was 6–7 meV, thus about 20% less than we get here.

The calculated magnitudes of the tunnel currents are also in reasonable agreement with the experiment. Improving the accuracy would at least require a more sophisticated calculation of the tunneling matrix element. Our calculated currents differ from the experimental ones in that the theoretical peak currents increase with increasing magnetic field. Most of this increase is caused by the prefactor $(1 - \nu)$ in the expression for the current, and the peak current variation with magnetic field can be reduced if correlations between the Wigner crystals are taken into account [see the discussion following Eq. (15)].

In Fig. 5, we display I-V curves for a number of different lattice parameters (different electron densities).[28] The peak voltage varies with a_0 roughly as $V_{\text{peak}} \sim 1/a_0$. This is to be expected since the peak originates from the Coulomb interaction between electrons. Moreover, it is at least in a qualitative agreement with experimental observations made when varying the electron density in one of the quantum wells.[2] Within our theory, the $1/a_0$ behavior can be found from a rather simple dimensional analysis as follows. The center of mass of the I-V spectrum, which approximately equals the peak position, is given by the polaron shift. Here we assume that $\Delta_L = 0$ (in all numerical calculations we have set the electron-magnetophonon matrix elements equal to zero in the initial state), so we concentrate on analyzing Δ_R, see Eq.

(20). An electron-magnetophonon matrix element is [see Eq. (B23)] the scalar product of the zero-point motion amplitude, here denoted by $\mathbf{u}_{\text{zero}}$, of the lattice electrons and a derivative of the Coulomb potential. The second of these factors scales as $1/a_0^2$. To get an estimate of the zero-point motion, we must keep in mind that the potential energy makes up for practically all of the zero-point energy of a magnetophonon. This gives us

$$\frac{\hbar\omega}{2} \approx \frac{1}{2}m^*\omega_T^2|\mathbf{u}_{\text{zero}}|^2. \tag{32}$$

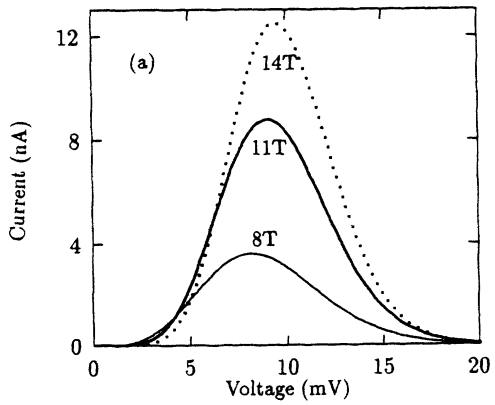

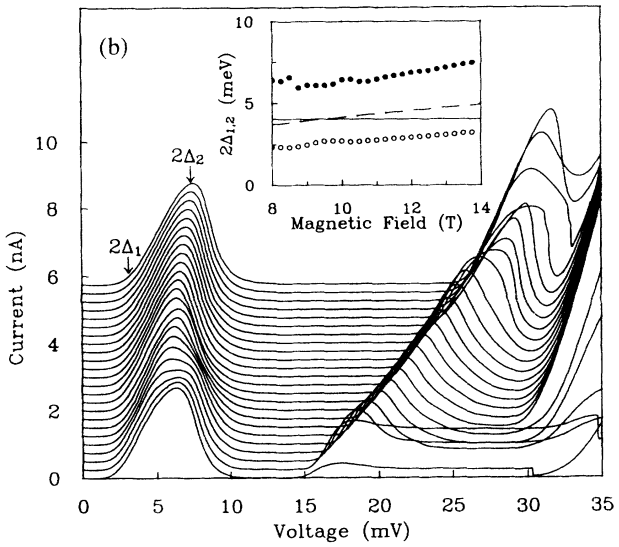

FIG. 4. Tunnel current as a function of voltage for different magnetic fields. (a) Theoretical results, the parameter values used in the calculations have been taken directly from the experiment (Ref. 2). The lattice parameter of the Wigner crystals a_0=270 Å corresponding to an electron density $n \approx 1.6 \times 10^{11}$ cm.$^{-2}$ The quantum well width was L= 200 Å, the barrier thickness d = 175 Å, and the total sample area was S = 0.0625 mm^2. The barrier height was V_b=250 meV. (b) Experimental results for a larger range of voltages from Ref. 2 (used with permission). The temperature was 0.6 K and the magnetic field was varied from 8 T to 13.75 T in steps of 0.25 T. The curves are vertically offset for clarity. Inset: Magnetic field dependence of onset ($2\Delta_1$) and peak ($2\Delta_2$) voltages. The solid line is the Coulomb energy $e^2/4\pi\epsilon\langle a\rangle$ while the dashed line is $0.4e^2/4\pi\epsilon l_c$.

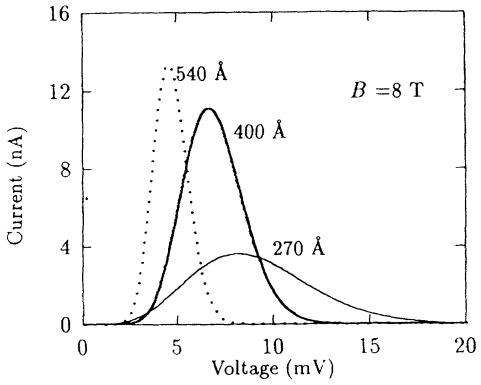

FIG. 5. Calculated tunnel current as a function of voltage for three different lattice parameters as indicated next to the curves. The magnetic field was 8 T. The peak voltage varies as $\sim 1/a_0$, and the peak width varies as $\sim 1/(a_0^2\sqrt{B})$.

As discussed earlier [see Eq. (6)] $\omega \sim 1/a_0^3B$, and $\omega_T^2 \sim 1/a_0^3$ because it is a measure of the restoring forces. This means that the square of the zero-point motion amplitude of an electron due to the magnetophonons behaves as

$$|\mathbf{u}_{\text{zero}}| \sim 1/\sqrt{B}. \tag{33}$$

The number of terms appearing in Eq. (20) is of course independent of a_0 and B. We, therefore, conclude that the polaron shift scales as

$$\Delta_R \sim \frac{[(1/\sqrt{B})(1/a_0^2)]^2}{1/a_0^3B} \sim 1/a_0, \tag{34}$$

in agreement with the above observation.

We also see that, as the lattice parameter is increased, the I-V curves become more and more sharply peaked. Thus, the effects of quantum fluctuations become less important; the electron systems behave to an increasing degree classically. Since the total energy lost to excitation of magnetophonons scales as $1/a_0$, while the energy of a single magnetophonon varies as $a_0^{-3}B^{-1}$, the total number of excited magnetophonons, $\mathcal{N}$, behaves as

$$\mathcal{N} \sim a_0^2B. \tag{35}$$

From a standard argument we know that the uncertainty in the number of excited magnetophonons is $\sim \sqrt{\mathcal{N}}$, which yields a peak width Γ scaling as

$$\Gamma \sim \sqrt{\mathcal{N}}\frac{1}{a_0^3B} \sim \frac{1}{a_0^2\sqrt{B}}. \tag{36}$$

The peak voltage in Fig. 4(a) increases with increasing magnetic field. This was also seen experimentally. The effect is somewhat more pronounced in the experiment [Fig. 4(b)]. In the leading-order dimensional analysis above, the peak voltage did not show any magnetic-field dependence. We have found that the calculated peak voltage does not change much with B for magnetic fields larger than 14 T when the other parameter values have the values used in Fig. 4(a).

Turning our attention to the low-voltage behavior of the I-V characteristics, one can deduce from Eq. (25)

that, provided the function $g(\Omega)$ is constant up to a certain frequency, the current will show power-law behavior $I \sim V^{g/(2\pi)-1}$ up to the corresponding voltage. In our case g is fairly constant over most of the range of magnetophonon frequencies. We typically find approximate power-law behavior for the current as a function of voltage up to a voltage corresponding to half the maximum magnetophonon frequency. The exponent varies with the magnetic field; it is ≈ 4.8 for $B = 8$ T and ≈ 7.0 for $B = 13$ T. Thus, changes of the magnetic field do not affect the total integral of the function $g(\Omega)$ too much, since this is the polaron shift

$$\Delta_R = \hbar \int_0^{\omega_{\max}} \frac{d\Omega}{2\pi} g(\Omega), \tag{37}$$

but it changes the value of $g(\Omega)$ which determines the power-law exponent. All the magnetophonon frequencies scale as $\sim 1/B$, so $g(\Omega)$ and the power-law exponent increase approximately linearly with B.

We should also point out that, partly due to the magnetophonon density of states resulting from the $q^{3/2}$ dispersion, g exhibits a $\Omega^{-1/3}$ singularity for very low frequencies (less than a few percent of $\omega_{\max}$). In practice, however, this does not affect our results very much, but the limiting behavior of the I-V characteristics is a function that vanishes faster than any power law for small V. In Appendix C, we analyze this in considerable detail. He, Platzman, and Halperin[11] found, using the theory presented in Ref. 12, the limiting behavior $I \sim e^{-V_0/V}$. From a theoretical point of view their results should be more reliable than ours for these low voltages. We cannot expect the Wigner-crystal model to give a completely correct description of the long-range correlations that are involved in the slow relaxation processes. The experimental I-V characteristics did not show activated behavior at low voltages, which may be due to effects of disorder.[29,30]

In connection with the above we wish to comment on a rather remarkable finding of Eisenstein, Pfeiffer, and West. Their measured I-V curves can be approximated by $I \sim e^{-V_0/V}$ to a very good accuracy from $\frac{1}{3}V_{\text{peak}}$ to $\frac{2}{3}V_{\text{peak}}$.[29] Thus, this happens for voltages that are large enough that the limiting behavior found by He, Platzman, and Halperin[11] may not be applicable,[31] and it turns out that their theoretical value for the parameter V_0 is some seven times larger than what is found experimentally. To see what kind of behavior our theory gives on the low-voltage side of the current peak we have plotted I on a logarithmic scale versus $1/V$ in Fig. 6. We see that while we cannot reproduce exactly the same behavior as in the experiment, our "average" V_0 does not differ too much from the experimental value.

When the temperature is raised the strong suppression of the conductance at small bias gradually disappears. This is caused by thermally excited magnetophonons that can assist tunneling. We refer to Fig. 3 of our earlier paper[4] for an illustration of how the differential conductance develops with increasing temperature. The conductance at zero voltage exhibits a thermally activated behavior, $(dI/dV)_{V=0} \sim e^{-T_A/T}$. This is illustrated in Fig. 7 for a few different values of the magnetic field. The activation temperatures we find are in rather good agreement with the experiment, and as in the experiment our activation temperatures are approximately proportional to the magnetic field.

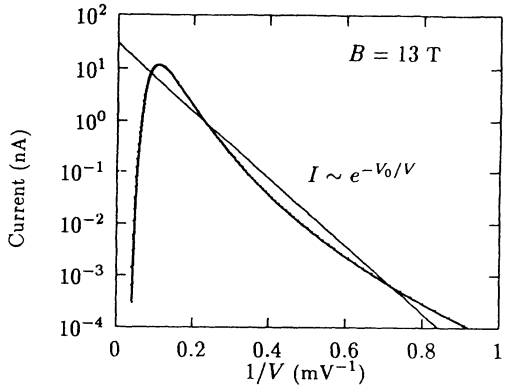

FIG. 6. The current on a logarithmic scale vs $1/V$. The thick curve shows our calculated results for $B = 13$ T, while the straight line corresponds to an "activated" I-V curve, $I \sim e^{-V_0/V}$ with $V_0 = 15$ mV. In the experiment (Ref. 29) this kind of activated behavior was found over a wide range of voltages, at $B = 13.5$ T the measured V_0 was ≈ 13.4 mV.

In view of our results for the low-voltage I-V characteristics (the approximate power law) this activated behavior is a bit surprising. Roughly speaking, it should not make any difference whether energy is supplied to the system by an external voltage source or by increasing the temperature. What appears to happen is that over the temperature range covered in Fig. 7, the major contributions to $(dI/dV)_{V=0}$ in Eq. (31) come from frequencies where $C_{\text{em}}(\omega) \sim e^{-\omega_0/\omega}$, i.e., the behavior illustrated in Fig. 6. In Fig. 7 we indeed see a tendency for the low-voltage conductance to decrease slower than the activated behavior at the low-temperature end of the diagram.

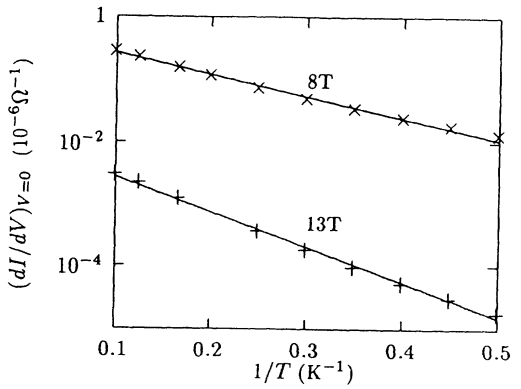

FIG. 7. Determination of the activation temperature for the zero-voltage differential conductance. The symbols are calculated values, while the straight lines give exactly activated behavior $(dI/dV)_{V=0} \sim e^{-T_A/T}$. To plot these lines we used $T_A = 8$ K for $B = 8$ T, and $T_A = 13$ K for $B = 13$ T.

IV. EFFECTS OF EXCITATIONS TO THE NEXT LANDAU LEVEL

So far we have only considered the effects of *magnetophonons*, which was sufficient to discuss the first peak of the I-V curve. Experimentally, another current maximum was observed at a voltage that was about $\hbar\omega_c/e$ higher than the voltage corresponding to the first peak, see Fig. 4(b). This suggests that at such high voltages transitions between Landau levels are important. In our model, we can include these transitions in two different ways: the tunneling electron can couple to the *magnetoplasmon* modes of the Wigner crystal, and the tunneling electron itself can be excited to the next Landau level. Coupling to magnetoplasmons can be included by extending the sums in Sec. III to run over the magnetoplasmon modes as well, but allowing for the excitation of the tunneling electron requires some changes in the formalism. In the end, it turns out that coupling to magnetoplasmons affects the results more than the single-particle excitations, but for completeness we consider them both. The new Hamiltonian, which includes both these effects, can be written as $H = H_L + H_R + H_T$. The Hamiltonian for one quantum well is given by $H_0 + H_1$, where (note that what we denote as $H_0 + H_1$ in this section corresponds to H_0 in the previous sections)

$$H_0 = \sum_\alpha \hbar\omega_\alpha a_\alpha^\dagger a_\alpha + \sum_n \varepsilon_n c_n^\dagger c_n,$$

$$H_1 = \sum_\alpha \left\{ \sum_{nm} (M_\alpha^{nm} a_\alpha + M_{-\alpha}^{nm} a_\alpha^\dagger) c_n^\dagger c_m \right\}. \tag{38}$$

The subscript α denotes, in addition to the wave vector and quantum well, also whether the bosonic excitation is a magnetophonon or a magnetoplasmon (cf. Appendix B), and the subscript n is the Landau level index of the tunneling electron (0 or 1). For compactness we have suppressed the quantum well index of the electron operators, and furthermore we have defined $(M_\alpha^{nm})^* \equiv M_{-\alpha}^{nm}$. The tunneling Hamiltonian is generalized to

$$H_T = \sum_{nm} T_{LR}^{nm} c_{Ln}^\dagger c_{Rm} + \text{H.c.}, \tag{39}$$

where we have explicitly shown also the quantum well index.

We proceed as in Sec. III and write the current as the Fourier transform of the correlation function between forward and backward tunneling. The Hamiltonian $H_L + H_R$ still falls in the category of exactly solvable independent-boson models, and we can repeat much of the previous analysis. It is useful to introduce a matrix notation so that

$$H_T = H_T^+ + H_T^- = \begin{pmatrix} c_{R0}^\dagger & c_{R1}^\dagger \end{pmatrix} \widehat{T}^+ \begin{pmatrix} c_{L0} \\ c_{L1} \end{pmatrix} + \begin{pmatrix} c_{L0}^\dagger & c_{L1}^\dagger \end{pmatrix} \widehat{T}^- \begin{pmatrix} c_{R0} \\ c_{R1} \end{pmatrix}. \tag{40}$$

The current-voltage characteristics are again given by

$$I(V) = (e/\hbar^2)[I^{-+}(eV/\hbar) - I^{+-}(-eV/\hbar)],$$

where $I^{-+}(t) = \langle H_T^-(t) H_T^+(0) \rangle$. The operators are in the Heisenberg picture and their time development is governed by $H_L + H_R$. In evaluating $I^{-+}(t)$ we formally regard H_1 as a perturbation, and calculate $I^{-+}(t)$ using the interaction picture. The time development of the "perturbation" H_1 is

$$H_1(t) = \sum_{nm} c_n^\dagger \sum_\alpha \mathcal{A}_\alpha^{nm}(t) c_m,$$

where $\widehat{\mathcal{A}}_\alpha(t)$ is the effective boson (magnetophonon and magnetoplasmon) operator

$$\mathcal{A}_\alpha^{nm}(t) = \left[M_{-\alpha}^{nm} e^{i\omega_\alpha t} a_\alpha^\dagger + M_\alpha^{nm} e^{-i\omega_\alpha t} a_\alpha \right] e^{i\omega_c (n-m)t}. \tag{41}$$

For simplicity we set the electron-boson couplings before the tunneling event to zero, since in the end this is what we do in the numerical calculations. In the interaction picture the time development of the operators is governed by H_0, and we find, after some rearrangements,

$$I^{-+}(t) = \sum_{nrs} \Bigg\{ e^{i(\varepsilon_{Ln} - \varepsilon_{Rr})t/\hbar} \times T_{nr}^- T_{sn}^+ \Big\langle c_{Ln}^\dagger c_{Ln} c_{Rr} c_{Rs}^\dagger c_{Rs} \times \left[\mathrm{T} \exp\left(-i \int_0^t \sum_\alpha \widehat{\mathcal{A}}_\alpha(t') \right) \right]_{rs} \Big\rangle \Bigg\}. \tag{42}$$

The "internal" electron operators that arise from the expansion of the time evolution operator appear in pairs like $c_{Rm} c_{Rm}^\dagger$, which only give a factor of unity and, therefore, do not contribute to the result. Consequently, products of the operators $H_1(t)$ have been replaced by matrix products of entirely bosonic operators. We can evaluate the remaining expectation values of fermion operators, which give $\langle L | c_{Ln}^\dagger c_{Ln} | L \rangle = \nu_{Ln}$ and $\langle R | c_{Rr} c_{Rr}^\dagger c_{Rs} c_{Rs}^\dagger | R \rangle = (1 - \nu_{Rr} - \nu_{Rs} + \delta_{rs}\nu_{Rr})$. Here we again assumed that the electron systems in the two wells are mutually uncorrelated. To avoid notational difficulties we limit the discussion from here on to diagonal tunneling matrices $\widehat{T}_{LR}$; the general case can be analyzed along the same lines. Physically, the off-diagonal elements of $\widehat{T}_{LR}$ are quite small due to the orthogonality of the in-plane wave functions. We have now reduced the expression (42) to a purely bosonic form. Following Mahan,[27] we find that the perturbation theory can be summed exactly to all orders using an exponential resummation, which yields

$$I^{-+}(t) = \mathrm{Tr} \Big\{ \exp\left[i(\hat{\varepsilon}_L - \hat{\varepsilon}_R)t/\hbar \right] \hat{\nu}_L (\hat{I} - \hat{\nu}_R) |\widehat{T}_{LR}|^2 \times \exp\left[-\sum_\alpha \hat{\phi}(\alpha, t) \right] \Big\}. \tag{43}$$

Here $\hat{\varepsilon}$ and $\hat{\nu}$ are diagonal matrices of the form $(\hat{\varepsilon}_L)_{nm} = \varepsilon_{Ln}\delta_{nm}$, $(\hat{\nu}_L)_{nm} = \nu_{Ln}\delta_{nm}$, and $\hat{I}$ is the unit matrix. The effect of inter-well correlations would be to increase the $(\hat{I} - \hat{\nu}_R)$ factor, as discussed in the previous section. We have furthermore defined $\hat{\phi}(\alpha,t)$ as a 2×2 matrix of double-time integrals,

$$\hat{\phi}(\alpha,t) = \frac{1}{2}\int_0^t dt_1 \int_0^t dt_2 \langle T\hat{\mathcal{A}}_\alpha(t_1)\hat{\mathcal{A}}_\alpha(t_2)\rangle. \tag{44}$$

We proceed by evaluating the double-time integrals to obtain the functions $\hat{\phi}(\alpha,t)$. The component $\phi^{(00)}$ is given by

$$\begin{aligned}\phi^{(00)}(\alpha,t) = M_\alpha^{(00)}M_{-\alpha}^{(00)}\frac{1}{\hbar^2\omega_\alpha^2}\left[(1+N_\alpha)(1-e^{-i\omega_\alpha t}) + N_\alpha(1-e^{i\omega_\alpha t}) - i\omega_\alpha t\right] \\ + \frac{1}{2\hbar^2}\left[M_\alpha^{(01)}M_{-\alpha}^{(10)} + M_\alpha^{(10)}M_{-\alpha}^{(01)}\right]\left[\frac{1+N_\alpha}{(\omega_\alpha+\omega_c)^2}(1-e^{-i(\omega_\alpha+\omega_c)t})\right. \\ \left. + \frac{N_\alpha}{(\omega_\alpha-\omega_c)^2}(1-e^{i(\omega_\alpha-\omega_c)t}) + i\frac{2N_\alpha}{\omega_\alpha^2-\omega_c^2}\omega_c t - i\frac{t}{\omega_\alpha+\omega_c}\right].\end{aligned} \tag{45}$$

The off-diagonal components can also be calculated straightforwardly, and we obtain somewhat more complicated expressions than (45). We have ignored thermal effects on the fermion system, which is justified at temperatures $k_BT \ll \hbar\omega_c$, when thermal transitions between Landau levels are suppressed. Consequently, the occupation numbers N_α are small for magnetoplasmons, and magnetoplasmon absorption processes are quite insignificant. An interesting feature of the result (45) is that the second term on the last line gives rise to a temperature-dependent polaron shift, due to the temperature dependence of the magnetophonon and magnetoplasmon occupation numbers N_α. However, this effect is very small due to the smallness of the off-diagonal couplings $M_\alpha^{(01)}$ and $M_\alpha^{(10)}$, and is, therefore, not likely to be measurable.

To obtain the current as a function of the applied voltage we must calculate the matrix Fourier transform of $\exp[-\sum_\alpha \hat{\phi}(\alpha,t)]$. Unfortunately, we cannot use the integral-equation approach since the various matrices do not commute, which makes it difficult to evaluate the necessary time derivative. Thus, in our numerical calculations we have just kept the contribution from $\phi^{(00)}(\alpha,t)$ in Eq. (43). Moreover, when evaluating the expression in Eq. (45) we have only kept the intra-Landau level matrix elements $M_\alpha^{(00)}$. We have found that the effects of the off-diagonal, inter-Landau level matrix elements are smaller in comparison. Consequently, in the numerical work we have included higher Landau level effects only through coupling to magnetoplasmons, as we have deemed this to be the most important contribution.

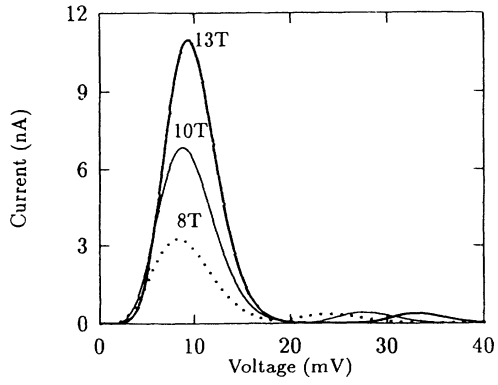

FIG. 8. Calculated tunnel current when the coupling to magnetoplasmons is taken into account. The magnitude of the magnetic field is indicated next to the curves, the rest of the parameter values are the same as in Fig. 4. The voltage difference between the two peaks roughly corresponds to the cyclotron energy.

The results of the calculations are presented in Fig. 8. The I-V characteristics display two peaks, the first of these is, as before, associated with magnetophonon shakeup, while the other one originates from a combination of magnetophonon shakeup and the emission of one magnetoplasmon. The two peaks are separated by a voltage corresponding to the cyclotron energy. This is basically in agreement with the experiment [Fig. 4(b)], even though the two peaks of the experimental I-V characteristics were a little closer together. This difference may, for example, be due to changes in the electron effective mass caused by the strong magnetic field. As for the relative amplitudes of the two peaks, our theory is not in very good agreement with the experiment. The second peak is too weak relative to the first one. In our calculation, the relative suppression of the second peak is primarily caused by the larger frequency denominators entering the function $g(\Omega)$ when dealing with magnetoplasmons. The discrepancy between theory and experiment in terms of relative peak strengths indicates that quantum-mechanical effects not included in our theory play a quite important role in the interactions causing transitions between Landau levels.

V. DISCUSSION

The most important question to ask when evaluating our theory is "How well can a Wigner crystal describe the real electron liquid?" As we have argued in Sec. II we think that the Wigner crystals give a rather good description of the short-range order of the real systems. These short-range interactions determine the primary en-

ergy scale in the problem, the amount of energy it takes to move an electron from one quantum well to the other. This sets the peak voltage, which our theory can predict rather well.

It is much more difficult to say how well the model describes the long-wavelength collective modes of the real system. A crucial feature of the model is that it supports collective modes of arbitrarily low frequencies. To get a suppression of the current at low voltages it is essential that the function $g(\Omega)$ is nonzero all the way down to $\Omega = 0$. In our model, this is achieved by the long-wavelength magnetophonons. In the real system the slow relaxation processes probably involve strongly damped oscillations.[12] Thus, we believe that the Wigner-crystal model is qualitatively correct in the long-wavelength limit in the sense that it contains a large number of low-energy excitations. The nature of these excitations is, however, most likely somewhat different in the real system.

The theory based on Wigner crystals works well in explaining the main features of the I-V characteristics. If, on the other hand, the experimental technique is further refined so that detailed information about the long-wavelength excitations of the 2D systems can be extracted we cannot expect our theory to give quantitatively correct predictions in that regime.

The theory we have presented is in many ways a classical one. We expect it to work best for small filling factors. At what filling fraction does our theory start to break down? An obvious upper limit is $\nu=1$ at which quantum effects not included in this theory must influence the results. In fact, one could argue that the theory should be modified for all filling fractions larger than 1/2. In the limit of a very strong magnetic field the lowest Landau level should exhibit particle-hole symmetry, i.e., a filling factor ν should be equivalent to a filling factor $(1-\nu)$ *at the same magnetic field.* However, we have not used such a symmetry here. The reason for this is twofold. First, it seems to us that imposing a quantum-mechanical symmetry on our, to a large extent, classical model would make up for a rather uncontrolled mixture of classical and quantum concepts. What we do now is more consistent. Moreover, in their experiment Eisenstein, Pfeiffer, and West[2] saw a reduction of the Coulomb blockade effect, in accord with the $1/a_0$ behavior we found above, when reducing the electron density at a constant magnetic field.

The effects of the magnetic field were less pronounced in the experiments of Ashoori *et al.*[1] than in the ones by Eisenstein, Pfeiffer, and West.[2] The major difference is that the differential conductance does not show a pseudogap in Ref. 1. One possible explanation of this is of course the lower electron mobility of the samples used in these experiments. Such an interpretation is supported by the calculation by Yang and MacDonald.[13] Another reason may be that Ashoori *et al.* studied tunneling between a 2D and a 3D system. Screening effects in the 3D system could reduce the coupling between the tunneling electron and the low-energy long-wavelength excitations, so that the x-ray edge behavior and the pseudogap are lost.

We conclude by discussing possible improvements of the calculation within the Wigner-crystal model. In this calculation we have neglected all interactions between electrons in different quantum wells. If such interactions were included we expect the peak voltage to decrease due to the interaction between the Wigner crystal to which the electron tunnels, and the hole left behind on the other side. We have calculated this hole contribution to the Madelung energy of the final state and found that it explains rather well the difference of ≈ 2 meV between the peak voltage we calculate and the one that was measured. To take this into account in the full calculation one should include the hole contribution when calculating the electron-magnetophonon matrix elements. At the same time, for consistency, the Wigner crystals should be allowed to interact mutually. This would modify the collective modes: acoustic and optical magnetophonons would appear.[28]

VI. SUMMARY

We have calculated the tunnel current between two two-dimensional electron systems in a strong perpendicular magnetic field. These 2D systems are strongly correlated since only the lowest Landau level is partially filled with electrons. Therefore, we have modeled them as Wigner crystals. When an electron tunnels from one Wigner crystal to the other, energy is released in the form of collective excitations, magnetophonons, and magnetoplasmons. It turns out that a large number of low-energy magnetophonons are created in a typical tunneling event. This is analogous to what happens when a core hole suddenly is created in an electron gas, and leads to a strongly suppressed tunnel current at low voltages. This pseudogap is followed by a peak in the tunnel current.

Our calculated I-V curves agree well with recent experimental results.[2] The peak voltage is approximately the same in both experiment and theory, and the low-voltage conductance shows the same kind of suppression in both. When the temperature is raised, the measured low-voltage conductance exhibits an activated behavior, with an activation temperature of the order of 10 K. Also here our theoretical results are in rather close agreement with the experiment. Finally, we have included effects of excitations to the next Landau level in our theory. This gives rise to a second peak in the I-V characteristics at a voltage $\hbar\omega_c/e$ above the first peak. This is in qualitative agreement with the experiment; however, the second peak was relatively stronger in the experiment than we find in our calculation.

ACKNOWLEDGMENTS

We have benefited from discussions with Karsten Flensberg, Antti-Pekka Jauho, and Henrik Smith. We are grateful to J. P. Eisenstein for allowing us to reproduce a figure showing the experimental results of Ref. 2.

APPENDIX A: THE DYNAMICAL MATRIX

In this appendix, we give a rapidly converging expression for the dynamical matrix. These calculations involve the Coulomb interaction and to evaluate the lattice sums we use the Ewald transformation in two dimensions.[16,32] This builds on two facts. First, the $1/r$ potential at a point $\mathbf{x}$ due to an electron at a lattice point $\mathbf{R}_i$ can be written as a Gaussian integral

$$\frac{1}{|\mathbf{x}-\mathbf{R}_i|}=\frac{2}{\sqrt{\pi}}\int_0^\infty d\eta e^{-\eta^2|\mathbf{x}-\mathbf{R}_i|^2}. \tag{A1}$$

Second, a sum of Gaussians over the direct lattice can be expressed as a sum over the reciprocal lattice. More precisely

$$\sum_i e^{-\eta^2|\mathbf{x}-\mathbf{R}_i|^2}e^{-i\mathbf{q}\cdot\mathbf{R}_i}=e^{-i\mathbf{q}\cdot\mathbf{x}}\sum_{\mathbf{G}}\frac{\pi}{S_0\eta^2}\exp\left(-\frac{|\mathbf{q}+\mathbf{G}|^2}{4\eta^2}\right)e^{-i\mathbf{G}\cdot\mathbf{x}}, \tag{A2}$$

where $\mathbf{G}$ is a reciprocal lattice vector and S_0 is the area of the unit cell of the direct lattice.

The dynamical matrix $\widehat{D}(\mathbf{q})$ is the Fourier transform of the force constants that one obtains when expanding the potential energy of the Wigner crystal to second order in the electron displacements away from equilibrium. A rapidly converging expression for $\widehat{D}(\mathbf{q})$ is found by using Eqs. (A1) and (A2), short-range interactions (large η) are summed over the direct lattice, while long-range interactions (small η) are summed over the reciprocal lattice. This yields the final expression for the elements of the dynamical matrix (the indices α and β denote directions, i.e., x or y)

$$\begin{aligned}D_{\alpha\beta}(\mathbf{q})=&\frac{e^2}{4\pi\epsilon m^*}\frac{2\xi^3}{\sqrt{\pi}}\sum_{\mathbf{R}_i\neq 0}\left[2\xi^2R_{\alpha i}R_{\beta i}\phi_{3/2}(\xi^2|\mathbf{R}_i|^2)-\delta_{\alpha\beta}\phi_{1/2}(\xi^2|\mathbf{R}_i|^2)\right]\left[1-\cos(\mathbf{q}\cdot\mathbf{R}_i)\right]\\&+\frac{e^2}{4\pi\epsilon m^*}\frac{\sqrt{\pi}}{\xi S_0}\sum_{\mathbf{G}\neq 0}\left[(q_\alpha+G_\alpha)(q_\beta+G_\beta)\phi_{-1/2}\left(\frac{|\mathbf{q}+\mathbf{G}|^2}{4\xi^2}\right)-G_\alpha G_\beta\phi_{-1/2}\left(\frac{|\mathbf{G}|^2}{4\xi^2}\right)\right]\\&+\frac{e^2}{4\pi\epsilon m^*}\frac{2\pi}{S_0}\frac{q_\alpha q_\beta}{|\mathbf{q}|}\operatorname{erfc}\left(\frac{|\mathbf{q}|^2}{4\xi^2}\right).\end{aligned} \tag{A3}$$

The Misra functions $\phi_m(x)$ appearing in this equation are defined by

$$\phi_m(x)=\int_1^\infty t^m e^{-xt}dt, \tag{A4}$$

and can be related to the complementary error function $\operatorname{erfc}(x)$. The parameter ξ separates small and large η values. In the numerical calculations we used $\xi=1.6/a_0$.

APPENDIX B: MAGNETOPHONON AND MAGNETOPLASMON QUANTIZATION

In this appendix, we quantize the magnetophonons and calculate explicit expressions for the electron-magnetophonon matrix elements. We must go through the following procedure in order to get a Hermitian electron-magnetophonon interaction, i.e., essentially find a way of expressing the electron displacements $\mathbf{u}_i$ as real quantities. This is not easily done starting from the classical magnetophonons and magnetoplasmons, since the Wigner-crystal electrons rotate in the same direction both when a $\mathbf{q}$ and a $-\mathbf{q}$ mode of the same kind propagates (cf. Fig. 2).

In the harmonic approximation the Hamiltonian for the Wigner crystal in a magnetic field $\mathbf{B}=B\hat{z}$, described by a vector potential $\mathbf{A}$ in the symmetric gauge, can be written as

$$\begin{aligned}H=&\frac{1}{2m^*}\sum_i\left[-i\hbar\nabla_i+e\mathbf{A}(\mathbf{r}_i)\right]^2\\&+\frac{1}{2}\sum_{i,j,\alpha,\beta}u_{\alpha i}f_{\alpha\beta}(\mathbf{R}_i,\mathbf{R}_j)u_{\beta j}.\end{aligned} \tag{B1}$$

Here $f_{\alpha\beta}(\mathbf{R}_i,\mathbf{R}_j)$ are the force constants of the Wigner crystal. The force constants are only a function of the difference between $\mathbf{R}_i$ and $\mathbf{R}_j$, and their Fourier transform is the dynamical matrix. We have omitted the constant in the expression for the potential energy. The electron coordinates $\mathbf{r}_i$ are given by $\mathbf{r}_i=\mathbf{R}_i+\mathbf{u}_i$. Since the vector potential is a linear function of the coordinates, we can write

$$\mathbf{A}(\mathbf{r}_i)=\mathbf{A}(\mathbf{R}_i)+\mathbf{A}(\mathbf{u}_i). \tag{B2}$$

We divide the Hamiltonian into two parts $H=H_0+H_B$, and define

$$\mathbf{p}_i=-i\hbar\nabla_i+e\mathbf{A}(\mathbf{R}_i). \tag{B3}$$

By writing

$$H_0=\frac{1}{2m^*}\sum_i\mathbf{p}_i^2+\frac{1}{2}\sum_{i,j,\alpha,\beta}u_{\alpha i}f_{\alpha\beta}(\mathbf{R}_i,\mathbf{R}_j)u_{\beta j}, \tag{B4}$$

all dynamic effects of the magnetic field are contained in H_B. The Hamiltonian H_0 can be diagonalized in a

standard way. We introduce the Fourier transforms of the electron momenta and displacements,

$$\mathbf{p}_i = \frac{1}{\sqrt{N}} \sum_{\mathbf{q}} \mathbf{P}_{\mathbf{q}}\, e^{-i\mathbf{q}\cdot\mathbf{R}_i}, \tag{B5}$$

and

$$\mathbf{u}_i = \frac{1}{\sqrt{N}} \sum_{\mathbf{q}} \mathbf{Q}_{\mathbf{q}}\, e^{i\mathbf{q}\cdot\mathbf{R}_i}, \tag{B6}$$

so that H_0 can be written as

$$H_0 = \frac{1}{2m^*} \sum_{\mathbf{q}} \mathbf{P}_{\mathbf{q}} \cdot \mathbf{P}_{-\mathbf{q}} + \frac{m^*}{2} \sum_{\mathbf{q},\alpha\beta} Q_{\mathbf{q}\alpha} D_{\alpha\beta}(\mathbf{q}) Q_{-\mathbf{q}\beta}. \tag{B7}$$

Next we diagonalize the dynamical matrix to find the eigenfrequencies $\omega_{T\mathbf{q}}$ and $\omega_{L\mathbf{q}}$ and the corresponding eigenvectors $\mathbf{e}_{T\mathbf{q}}$ and $\mathbf{e}_{L\mathbf{q}}$. By introducing phonon creation and annihilation operators for the Wigner crystal in the absence of a magnetic field through

$$b_{T\mathbf{q}} = \frac{1}{\sqrt{2\hbar}} \left(\sqrt{m^*\omega_{T\mathbf{q}}}\, \mathbf{Q}_{\mathbf{q}} + \frac{i}{\sqrt{m^*\omega_{T\mathbf{q}}}} \mathbf{P}_{\mathbf{q}} \right) \cdot \mathbf{e}_{T\mathbf{q}}, \tag{B8}$$

etc., we get, neglecting the zero-point energy,

$$H_0 = \sum_{\mathbf{q}} (\hbar\omega_{T\mathbf{q}} b^\dagger_{T\mathbf{q}} b_{T\mathbf{q}} + \hbar\omega_{L\mathbf{q}} b^\dagger_{L\mathbf{q}} b_{L\mathbf{q}}). \tag{B9}$$

At this point, we can express the $\mathbf{A}\cdot\mathbf{p}$ terms and $\mathbf{A}^2$ terms in H_B in terms of the creation and annihilation operators. If we restrict our attention to the wave vectors in one-half the Brillouin zone, and introduce the notation

$$b_1 = b_{T\mathbf{q}}, \quad b_2 = b_{L\mathbf{q}}, \quad b_3 = b_{T-\mathbf{q}}, \quad b_4 = b_{L-\mathbf{q}}, \tag{B10}$$

we find that the full Hamiltonian takes the general form

$$H = \sum_{\mathbf{q}}{}' \Big(\sum_{\gamma\delta} L_{\gamma\delta} b^\dagger_\gamma b_\delta + \frac{1}{2} \sum_{\gamma\delta} [K_{\gamma\delta} b^\dagger_\gamma b^\dagger_\delta + K^*_{\gamma\delta} b_\gamma b_\delta] \Big). \tag{B11}$$

The prime on the sum over wave vectors indicates that it should be restricted to one-half the Brillouin zone. The 4×4 matrices $\widehat{L}$ and $\widehat{K}$ have the block structure

$$\widehat{L} = \begin{bmatrix} \widehat{B}_L & 0 \\ 0 & \widehat{B}_L \end{bmatrix} \tag{B12}$$

and

$$\widehat{K} = \begin{bmatrix} 0 & \widehat{B}_K \\ \widehat{B}_K & 0 \end{bmatrix}. \tag{B13}$$

The blocks $\widehat{B}_L$ and $\widehat{B}_K$ are given by

$$\widehat{B}_L = \begin{bmatrix} \hbar\omega_T + \frac{\hbar\omega_c^2}{8\omega_T} & -i\frac{\hbar\omega_c}{4}\sqrt{\frac{\omega_T^2+\omega_L^2}{\omega_T\omega_L}} \\ i\frac{\hbar\omega_c}{4}\sqrt{\frac{\omega_T^2+\omega_L^2}{\omega_T\omega_L}} & \hbar\omega_L + \frac{\hbar\omega_c^2}{8\omega_L} \end{bmatrix}, \tag{B14}$$

and

$$\widehat{B}_K = \begin{bmatrix} \frac{\hbar\omega_c^2}{8\omega_T} & i\frac{\hbar\omega_c}{4}\sqrt{\frac{\omega_L^2-\omega_T^2}{\omega_T\omega_L}} \\ i\frac{\hbar\omega_c}{4}\sqrt{\frac{\omega_L^2-\omega_T^2}{\omega_T\omega_L}} & \frac{\hbar\omega_c^2}{8\omega_L} \end{bmatrix}. \tag{B15}$$

The Hamiltonian (B11) can be diagonalized by a canonical transformation.[19] We define (for each $\mathbf{q}$) new operators a_α through

$$a_\alpha = \sum_\gamma u_{\alpha\gamma} b_\gamma - v_{\alpha\gamma} b^\dagger_\gamma. \tag{B16}$$

The inverse of this is

$$b_\gamma = \sum_\alpha u^*_{\alpha\gamma} a_\alpha + v_{\alpha\gamma} a^\dagger_\alpha. \tag{B17}$$

The Hamiltonian now takes the form

$$H = \sum_{\mathbf{q}}{}' \sum_\alpha \hbar\omega_\alpha a^\dagger_\alpha a_\alpha. \tag{B18}$$

The transformation coefficients $u_{\alpha\gamma}$ (not to be confused with the electron displacements) and $v_{\alpha\gamma}$ must satisfy the conditions

$$\sum_\gamma [u_{\alpha\gamma} u^*_{\beta\gamma} - v_{\alpha\gamma} v^*_{\beta\gamma}] = \delta_{\alpha\beta}, \tag{B19}$$

and

$$\sum_\gamma [u_{\alpha\gamma} v_{\beta\gamma} - v_{\alpha\gamma} u_{\beta\gamma}] = 0. \tag{B20}$$

We determine these coefficients by evaluating $[a_\alpha, H] = \hbar\omega_\alpha a_\alpha$ from Eqs. (B16) and (B11). In matrix notation this yields,

$$\left[\hbar\widehat{\omega} - \widehat{L}^* + \widehat{K}^* (\hbar\widehat{\omega} + \widehat{L})^{-1} \widehat{K}\right] \mathbf{u} = 0, \tag{B21}$$

and

$$\mathbf{v} = -(\hbar\widehat{\omega} + \widehat{L})^{-1} \widehat{K}\mathbf{u}. \tag{B22}$$

In these equations $\widehat{\omega}$ denotes a diagonal 4×4 matrix with the new eigenvalues ω_α as matrix elements. These frequencies are determined by the fact that in order to get nontrivial solutions the determinant of the matrix multiplying $\mathbf{u}$ in Eq. (B21) must vanish. Not surprisingly, one finds that two of the eigenfrequencies are identical to the classical magnetophonon frequency, while the other two equal the classical magnetoplasmon frequency.

The whole point in performing the canonical transformation above is that we now can write down explicit expressions for the electron-magnetophonon (and electron-magnetoplasmon) matrix elements. The interaction energy between an added electron at a point $\mathbf{x}$ and the electrons of the Wigner crystal is

$$\frac{e^2}{4\pi\epsilon}\sum_i \frac{1}{|\mathbf{x}-\mathbf{R}_i-\mathbf{u}_i|}.$$

To find the matrix elements M_α, we expand this expression to linear order in the displacements $\mathbf{u}_i$, and drop the Madelung energy contribution which is independent of the displacements. By using Eqs. (B6), (B8), and (B17) we can write the electron-magnetophonon interaction on the form used in the main text

$$H_{\text{el-mp}} = \frac{e^2}{4\pi\epsilon}\sum_i \mathbf{u}_i\cdot\frac{\mathbf{x}-\mathbf{R}_i}{|\mathbf{x}-\mathbf{R}_i|^3} = \sum_{\mathbf{q}}{}' \sum_\alpha M_{\alpha\mathbf{q}} a_{\alpha\mathbf{q}} + M^*_{\alpha\mathbf{q}} a^\dagger_{\alpha\mathbf{q}}, \tag{B23}$$

where

$$M_{\alpha\mathbf{q}} = \frac{e^2}{4\pi\epsilon\sqrt{Nm^*}}\left[\sqrt{\frac{\hbar}{2\omega_{T\mathbf{q}}}}(\mathbf{e}_{T\mathbf{q}}\cdot\mathbf{S}_\mathbf{q})(u^*_{\alpha1}+v^*_{\alpha3}) + \sqrt{\frac{\hbar}{2\omega_{L\mathbf{q}}}}(\mathbf{e}_{L\mathbf{q}}\cdot\mathbf{S}_\mathbf{q})(u^*_{\alpha2}+v^*_{\alpha4})\right.$$
$$\left.+\sqrt{\frac{\hbar}{2\omega_{T-\mathbf{q}}}}(\mathbf{e}_{T-\mathbf{q}}\cdot\mathbf{S}_{-\mathbf{q}})(u^*_{\alpha3}+v^*_{\alpha1}) + \sqrt{\frac{\hbar}{2\omega_{L-\mathbf{q}}}}(\mathbf{e}_{L-\mathbf{q}}\cdot\mathbf{S}_{-\mathbf{q}})(u^*_{\alpha4}+v^*_{\alpha2})\right]. \tag{B24}$$

In this expression $\mathbf{S}_\mathbf{q}$ denotes the lattice sum

$$\mathbf{S}_\mathbf{q} = \sum_i e^{i\mathbf{q}\cdot\mathbf{R}_i}\frac{\mathbf{x}-\mathbf{R}_i}{|\mathbf{x}-\mathbf{R}_i|^3}. \tag{B25}$$

It can be transformed into a rapidly converging sum using the methods discussed in Appendix A,

$$\mathbf{S}_\mathbf{q} = \frac{2}{\sqrt{\pi}}\xi^3\sum_{\mathbf{R}_i} e^{i\mathbf{q}\cdot\mathbf{R}_i}(\mathbf{x}-\mathbf{R}_i)\phi_{1/2}(\xi^2|\mathbf{x}-\mathbf{R}_i|^2) - \frac{2\pi i}{S_0}\sum_{\mathbf{G}}\frac{\mathbf{q}-\mathbf{G}}{|\mathbf{q}-\mathbf{G}|}e^{i(\mathbf{q}-\mathbf{G})\cdot\mathbf{x}}\operatorname{erfc}\left(\frac{|\mathbf{q}-\mathbf{G}|}{2\xi}\right). \tag{B26}$$

When calculating the matrix element due to the removal of an electron from a Wigner crystal, $\mathbf{x}=\mathbf{0}$, and the interaction with the electron at $\mathbf{R}_i=\mathbf{0}$ should not be included. This cancels the term $\mathbf{R}_i=\mathbf{0}$ in the sum above.

APPENDIX C: LOW-VOLTAGE BEHAVIOR

To determine the current-voltage characteristics of the system, we must find the Fourier transform $C(\omega)$. This can be done using the integral equation approach introduced by Minnhagen.[24] We analyze the integral equation

$$\omega C(\omega) = \beta\int_0^\omega \frac{d\Omega}{2\pi}(\omega-\Omega)^\alpha C(\Omega), \tag{C1}$$

which is the low frequency limit of Eq. (25), if we identify $\beta\Omega^\alpha$ with the low frequency behavior of $g(\Omega)$. In the end we will primarily be interested in the case $\alpha=-1/3$. To determine the low frequency behavior we use an *ansatz* of the form $C(\omega)=\omega^q e^{r\omega^s}$, where $r<0$ and $s<0$. By introducing the new variable $x=[(\Omega/\omega)^s-1]$ we can write the integral equation as

$$1 = -\frac{\beta}{2\pi s}\omega^\alpha\int_0^\infty dx[1-(1+x)^{1/s}]^\alpha(1+x)^{\frac{q+1}{s}-1}e^{r\omega^s x}. \tag{C2}$$

Since $r<0$ and $s<0$, for low enough frequencies ω^s is large and the exponential dies off very rapidly for $x>0$. Consequently, the main contribution comes from small x, and we can expand the binomials to second lowest order in x. By identifying the leading powers of ω we find for $0>\alpha>-1$

$$\begin{aligned} s &= \frac{\alpha}{\alpha+1},\\ r &= \frac{\alpha+1}{\alpha}[\beta\Gamma(\alpha+1)/(2\pi)]^{1/(\alpha+1)},\\ q &= -\frac{1}{2}\frac{\alpha+2}{\alpha+1}. \end{aligned} \tag{C3}$$

Thus, for $\alpha=-1/3$ we have

$$C(\omega) = \frac{1}{\omega^{5/4}}e^{-2[\beta\Gamma(2/3)/(2\pi)]^{3/2}\omega^{-1/2}}. \tag{C4}$$

In comparison, the value $\alpha=-1/2$ would give rise to an activated behavior $C(\omega)=\omega^{-3/2}e^{-\beta^2/(4\pi\omega)}$.[11,31] Note that the case $\alpha=0$ requires special handling, and can be shown to yield $C(\omega)=\omega^{\beta/(2\pi)-1}$.

[1] R. C. Ashoori, J. A. Lebens, N. P. Bigelow, and R. H. Silsbee, Phys. Rev. Lett. **64**, 681 (1990); Phys. Rev. B **48**, 4616 (1993).
[2] J. P. Eisenstein, L. N. Pfeiffer, and K. W. West, Phys. Rev. Lett. **69**, 3804 (1992).
[3] For a review, see *Single Charge Tunneling*, edited by H. Grabert and M. H. Devoret (Plenum, New York, 1992).
[4] P. Johansson and J. M. Kinaret, Phys. Rev. Lett. **71**, 1435 (1993).
[5] P. W. Anderson, Phys. Rev. Lett. **18**, 1049 (1967).

[6] A somewhat related orthogonality catastrophe has been discussed in connection with transport through a quantum dot in a strong magnetic field, see J. M. Kinaret, Y. Meir, N. S. Wingreen, P. A. Lee, and X.-G. Wen, Phys. Rev. B **46**, 4681 (1992).
[7] A. A. Odintsov, Zh. Eksp. Teor. Fiz. **94**, 312 (1988) [Sov. Phys. JETP **67**, 1265 (1988)].
[8] M. H. Devoret, D. Esteve, H. Grabert, G.-L. Ingold, H. Pothier, and C. Urbina, Phys. Rev. Lett. **64**, 1824 (1990).
[9] S. M. Girvin, L. I. Glazman, M. Jonson, D. R. Penn, and M. D. Stiles, Phys. Rev. Lett. **64**, 3183 (1990); K. Flensberg, S. M. Girvin, M. Jonson, D. R. Penn, and M. D. Stiles, Phys. Scr. **T42**, 189 (1992).
[10] Y. Hatsugai, P.-A. Bares, and X. G. Wen, Phys. Rev. Lett. **71**, 424 (1993).
[11] S. He, P. M. Platzman, and B. I. Halperin, Phys. Rev. Lett. **71**, 777 (1993).
[12] B. I. Halperin, P. A. Lee, and N. Read, Phys. Rev. B **47**, 7312 (1993).
[13] S.-R. E. Yang and A. H. MacDonald, Phys. Rev. Lett. **70**, 4110 (1993).
[14] A. L. Efros and F. G. Pikus, Phys. Rev. B **48**, 14694 (1993).
[15] P. Johansson, Phys. Rev. B **48**, 8938 (1993), and references therein.
[16] L. Bonsall and A. A. Maradudin, Phys. Rev. B **15**, 1959 (1977).
[17] R. Côté and A. H. MacDonald, Phys. Rev. Lett. **65**, 2662 (1990); Phys. Rev. B **44**, 8759 (1991).
[18] G. Rickayzen, *Green's Functions and Condensed Matter* (Academic, London, 1980), Chap. 7.
[19] N. N. Bogoliubov, *Lectures on Quantum Statistics* (Gordon and Breach, New York, 1967), pp. 213–220; A. S. Davydov, *Quantum Mechanics* 2nd ed. (Pergamon, Oxford, 1976), pp. 203–204. Note that Eqs. (52.31) and (52.29) of this reference contain printing errors; we give the corrected expressions in Eqs. (B22) and (B17), respectively.
[20] J. Bardeen, Phys. Rev. Lett. **6**, 57 (1961).
[21] M. Büttiker and R. Landauer, Phys. Rev. Lett. **49**, 1739 (1982).
[22] B. N. J. Persson and A. Baratoff, Phys. Rev. B **38**, 9616 (1988).
[23] G. D. Mahan, Phys. Rev. **163**, 612 (1967); P. Nozières and C. T. De Dominics, *ibid.* **178**, 1097 (1969); D. C. Langreth, Phys. Rev. B **1**, 471 (1970).
[24] P. Minnhagen, Phys. Lett. **56A**, 327 (1976).
[25] A. A. Lucas and M. Šunjić, Phys. Rev. Lett. **26**, 229 (1971).
[26] N. S. Wingreen, K. W. Jacobsen, and J. W. Wilkins, Phys. Rev. Lett. **61**, 1396 (1988); Phys. Rev. B **40**, 11834 (1989); M. Jonson, *ibid.* **39**, 5924 (1989).
[27] G. D. Mahan, *Many-Particle Physics* (Plenum, New York, 1990), pp. 285–324.
[28] For the largest lattice parameters used in these calculations one should ideally probably consider a model in which the two Wigner crystals are correlated and possess coupled collective modes. See, for example, X. M. Chen and J. J. Quinn, Phys. Rev. B **47**, 3999 (1993); V. I. Falko, Phys. Rev. B **49**, 7774 (1994).
[29] J. P. Eisenstein, L. N. Pfeiffer, and K. W. West, Surf. Sci. **305**, 393 (1994).
[30] J. P. Eisenstein (private communication).
[31] B. I. Halperin (private communication).
[32] M. Born and K. Huang, *Dynamical Theory of Crystal Lattices* (Clarendon, Oxford, 1954).

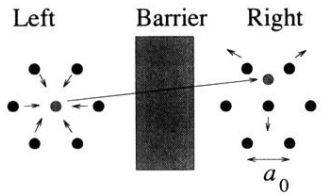

FIG. 1. Schematic picture of a tunneling event in our model. An electron starts from a lattice position in one of the triangular Wigner crystals (for clarity these have been depicted in a top view) and ends up in an interstitial position on the other side of the barrier. The surrounding electrons experience a sudden change in the potential and as a result relaxation processeses take place in the electron systems on both sides of the barrier. In our model the energy released in these relaxation processes is carried away mainly in the form of magnetophonons.